Surface charging of dielectric barriers under positive lightning impulse stress

Hans Kristian Meyer, Frank Mauseth, Martine Husøy
Norwegian University of Science and Technology
Department of Electric Power Engineering
Trondheim, Norway

Atle Pedersen
SINTEF Energy Research
Trondheim, Norway

***Abstract*—The complex geometry of gas-insulated substations makes it difficult to predict withstand voltages. A key challenge is the characterization of the interaction between electrical discharges and dielectric surfaces. A 60 mm rod-plane air gap with a dielectric barrier is stressed with positive lightning impulse, initiating discharges that are characterized with a PMT, a current measurement system and a high-speed camera. The discharges do not lead to breakdown at the tested voltages. The residual potential on the barrier is measured with a potential probe. Depending on the gap distance, the potential distribution is either bell-shaped or saddle-shaped. The saddle-shape appears when back discharges are seen from the electrode to the barrier. Back discharges reduce the surface charge until the voltage between barrier and rod is lower than the rod inception voltage. Charge density distributions are estimated from the measurements using FEM simulations. In addition to streamer discharges, leader-type channels are sometimes observed. They are arrested close to the dielectric surface. Streamers from these channels charge the dielectric barrier additionally.**

I. Introduction

Dielectric surfaces are common in medium voltage (MV) switchgear insulation systems, as e.g. spacers or shafts or as dielectric barriers. Proper use of gas-solid hybrid insulation techniques could offer the possibility to eliminate the need for the strong greenhouse gas SF_6 as insulating medium in MV switchgear. The increase in withstand strength can be realized by either covering parts of the electrodes [1]–[6] or with inter-electrode barriers [7]–[10]. Such methods require simulation models that model the relevant effects with high accuracy. The dielectric barrier influences the withstand strength by both increasing the shortest discharge path through the gas phase and by altering the field distribution due to surface charge.

The charging of dielectrics during positive lightning impulse (LI) has been studied by several researchers [1], [2], [6], [11]–[14]. Non-contacting field-nullifying probes offer the possibility to measure surface potential without influencing the measurement significantly [15], [16].

Previous work by the authors [9] documented the spatiotemporal propagation of positive streamers in a rod-plane gap with a dielectric barrier. The aim of this work is to further explore the characteristics of electrical discharges in an inhomogeneous air gap with a dielectric barrier. The focus is on the charge accumulation on the barrier surface during positive LI.

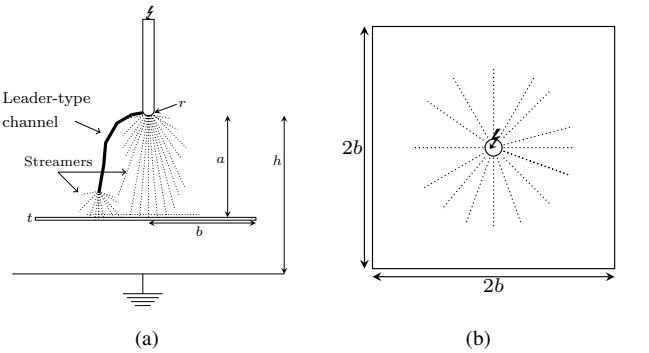

Fig. 1. Streamers and a leader-type channel in a h mm rod-plane gap reaching a dielectric barrier of thickness t, overhang b, at a distance a mm from the rod, seen from a) the side and b) above

II. Breakdown of air gaps with dielectric barriers

A. Breakdown mechanisms of inhomogeneous air gaps

Strongly inhomogeneous air gaps have inception levels below breakdown levels. Typically, the discharge starts with streamers that can easily cross the gap, leaving behind positive charges that influence the subsequent discharge development [17], [18].

Breakdown can occur after the primary streamer discharges by either channel-heating breakdown or leader-type channel breakdown [18], [19]. Channel-heating breakdown requires crossing and sufficient heating of a secondary streamer channel. These conditions can be met in gaps of a few cm if the voltage is high enough.

B. Streamer-dielectric interaction under impulse voltages

Streamers can propagate from the rod around the barrier to ground without causing breakdown. They propagate along the barrier and charge it (fig. 1), changing the field distribution and the following discharge development [9].

The field from these charges can cause discharges from the rod to the barrier or from the barrier to the rod at the impulse tail. These back discharges will alter the charge distribution on the surface, typically resulting in a saddle-shaped surface potential [20].

The residual charge will also influence the discharge development under following impulses. Charge of the same polarity

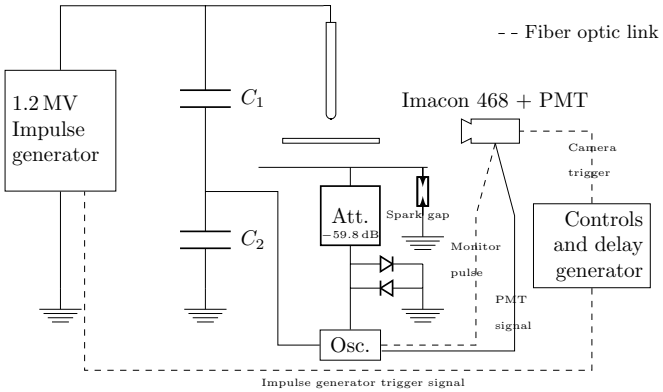

Fig. 2. Experimental set-up for studying discharge behaviour in a $h = 60\,\mathrm{mm}$ rod-plane gap with a dielectric barrier. Impulse generator, camera, PMT, current measurement using attenuators (Att.) and current measurement protection (spark gaps and diodes) are shown.

as the applied voltage will typically increase inception levels and reduce them for opposite polarity.

III. Method

A. Camera and PMT

A rod-plane gap with a hemispheric aluminium rod tip of radius $r_\mathrm{r} = 3.5\,\mathrm{mm}$ placed $h = 60\,\mathrm{mm}$ over a $1 \times 1\,\mathrm{m}$ ground plane and $a = 0$–$55\,\mathrm{mm}$ over a $600 \times 600 \times 5\,\mathrm{mm}$ polycarbonate barrier was stressed with $1.2/50\,\mu\mathrm{s}$ positive lightning impulses using an $1.2\,\mathrm{MV}$ impulse generator (see fig. 1 and fig. 2). The applied impulse levels $U = 50$–$70\,\mathrm{kV}$ were above streamer inception levels, but below breakdown levels. The experiments were performed in ambient air with the temperature, pressure and relative humidity being logged. An Imacon 468 ICCD camera with 7 frames of minimum exposure time $10\,\mathrm{ns}$ each was triggered with a delay generator to capture the spatiotemporal discharge development. An 85 mm f/1.8 Nikkor lens was used with the camera which was placed inside a Faraday cage about $1\,\mathrm{m}$ away from the rod. A continuous signal of the light intensity was obtained using a PMT about $2\,\mathrm{m}$ away. A Philips 56UVP/TVP PMT with different light filters was used with $2.5\,\mathrm{kV}$ supply voltage.

B. Current measurement system

The current was measured through a $23\,\mathrm{m}$ $50\,\Omega$ signal cable (RG-214) with bandwidth of about $400\,\mathrm{MHz}$ connected to the ground plane. The signal cable was matched at the oscilloscope end after passing through a series of $13\,\mathrm{GHz}$ T-type attenuators with a damping of up to $59.8\,\mathrm{dB}$. To protect the oscilloscope from breakdown currents, a $430\,\mathrm{V}$ spark gap was placed close to the ground plane, see fig. 2. Two diodes were placed in anti-parallel close to the oscilloscope to arrest the fastest voltage transients. The spark gap voltage or attenuation can be modified to measure different current ranges, but a practical upper limit is given by the thermal rating of the first attenuator, $5000\,\mathrm{V}$ for $400\,\mathrm{ns}$.

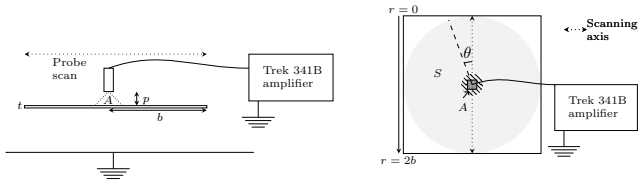

(a) (b)

Fig. 3. Charge measurement setup seen from a) the side and b) above. Area A seen by the probe depends on the fixed probe-to-surface distance p. The probe is supplied by a $20\,\mathrm{kV}$ amplifier and is scanned along the $2b = 600\,\mathrm{mm}$ long surface $S = \pi b^2$. The surface charge density distribution is estimated from the measured potential distribution with a FEM 2D axisymmetric model.

C. Digital post-processing

The propagation times in the PMT, current and voltage measurement cables were found using a pulse generator. These cable delays and the internal PMT delay were compensated in the digital post-processing of the $5\,\mathrm{GS\,s^{-1}}$ oscilloscope recordings. The correct timing of the camera monitor pulse was found using a PMT and a fast light-emitting diode. A Python script that filters out the current measurement noise and capacitive current was made. The script subtracts a scaled measurement where no discharge activity was seen in the gap by the camera and PMT. The original current measurement is also plotted in the results.

As the discharges are faint, the image brightness and contrast were enhanced with photo-editing software. These parameters were adjusted to the same levels in all image series to normalise the evaluation of discharge intensity. However, the different ICCDs have somewhat different gain. Images of background light were subtracted to normalise intensities of the ICCDs.

D. Charge measurement

A Trek 3455ET probe was used with a $20\,\mathrm{kV}$ Trek 341B high voltage amplifier to measure surface potential $U_\mathrm{S}(r)$, see fig. 3. The probe zeroes the electric field between itself and the surface by adjusting its potential. After the impulse, the rod was removed and the probe was positioned $p = 10\,\mathrm{mm}$ above the barrier surface and scanned along a single axis intersecting the rod position with steps of $\Delta r = 10\,\mathrm{mm}$. The probe was calibrated by placing it over the grounded plane and zeroing it. The barrier was then cleaned with isopropyl alcohol, resulting in a surface potential magnitude below $300\,\mathrm{V}$.

Local potential differences smaller than the surface A seen by the probe are not resolved [21]. If it is assumed that A extends approximately $45°$ from the circular probe aperture with radius $r_\mathrm{p} = 0.76\,\mathrm{mm}$, A is a circle with radius $r_A = 10.76\,\mathrm{mm}$ when the probe spacing is $p = 10\,\mathrm{mm}$. Potential variations over distances smaller than $2r_A \approx 21.5\,\mathrm{mm}$ are therefore not resolved.

E. Estimation of surface charge

Determining the surface charge density distribution $\rho(r, \theta)$ on the surface S (see fig. 3b) from a series of potential

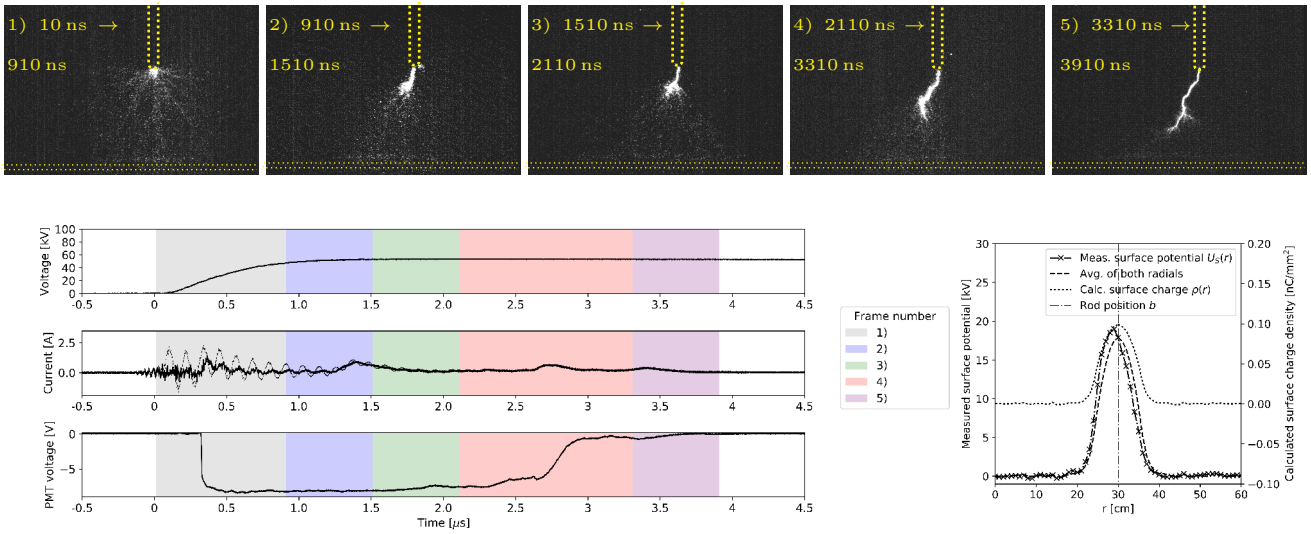

(a) Streamer discharges and leader-type channel development images, oscilloscope recordings and surface potential measurement, $h-a=5\,\mathrm{mm}$, $U=54.3\,\mathrm{kV}$. No breakdown occurred. PMT wavelength detection range 180–610 nm. Atmospheric pressure 1.014 bar, 21 °C, relative humidity 34 %.

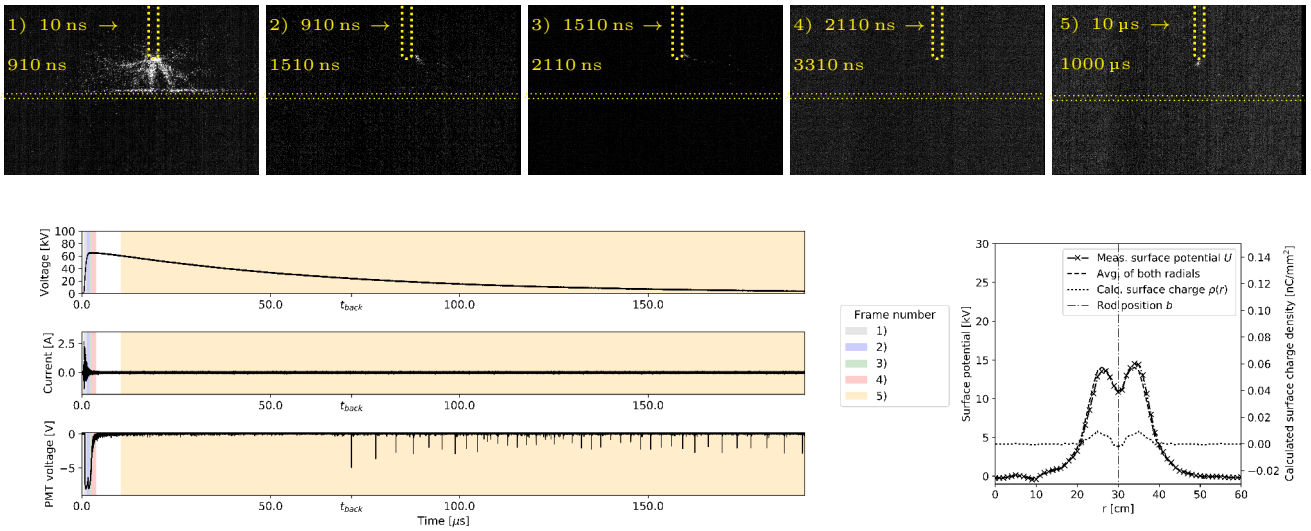

(b) Streamer discharge images, oscilloscope recordings and surface potential measurement, $h-a=40\,\mathrm{mm}$, $U=66.01\,\mathrm{kV}$. No breakdown occurred. PMT wavelength detection range 180–610 nm. Back discharges seen in last frame 5. Atmospheric pressure 1.005 bar, 22 °C, relative humidity 36 %.

Fig. 4. Discharge development and surface potential in $h=60\,\mathrm{mm}$ rod-plane gaps with a $600\times600\times5\,\mathrm{mm}$ dielectric barrier

measurements requires solving an inverse problem [22]. One way to solve it is to apply the measured potential distribution as a boundary condition on the dielectric surface in FEM software [23]. From Gauss' law, $\rho(r,\theta)$ is

$$\rho(r,\theta)=D_{\mathrm{n,gas}}(r,\theta)-D_{\mathrm{n,diel.}}(r,\theta) \tag{1}$$

If the surface charge distribution is assumed to be rotationally symmetric, 2D axisymmetric FEM calculations can be used. In the simulations, $\epsilon_r=3$ for the polycarbonate barrier was used [24]. The average measured potential of the two radials $r=b$ to $r=2b$ and $r=b$ to $r=0$ (fig. 3b) was applied to the barrier. In addition to the surface charge distribution $\rho(r)$, the total charge on the surface $Q_\mathrm{S}=\int_S\rho(r)\mathrm{d}S$ was estimated.

Error sources with this method include

1) *Non-symmetrical surface potential distribution*
2) *Resolution/interpolation errors*
3) *Measurement errors* – inaccurate probe stepping and probe-to-surface distance, unparallel probe and surface, and inherent probe errors [15], [16], [25].
4) *Non-zero initial surface potential*

IV. Results

A. Discharge development

Fig. 4a and 4b show discharge development in rod-plane gaps with barriers. Images, oscilloscope plots of voltage, current and PMT, measured surface potential after the discharge and calculated surface charge densities are shown. Color-shaded areas indicate the timing of the camera frames.

1) Leader-type channel: In fig. 4a, a leader-type channel propagates about $75\,\%$ of the gap length after the initial streamers in frame 1. Streamers propagate from the channel head to the barrier as depicted in fig. 1. The leader-type channel is arrested right above the barrier during frame 5.

2) Back discharges: In fig. 4b, the barrier surface is at $h - a = 40\,\mathrm{mm}$. In addition to primary streamer activity (frame 1), back discharges are observed at the impulse tail (frame 6). In the PMT voltage plot, these back discharges can be seen as a series of about 35 pulses spaced 3–6 µs starting at a time t_{back} when the applied voltage is around $U(t_{\mathrm{back}}) = 24\,\mathrm{kV}$, $37\,\%$ of peak voltage U. The interval shortens as the voltage decreases before increasing again from $150\,\mu\mathrm{s}$. The current amplitude is around $1\text{–}5\,\mathrm{mA}$, with rise and fall times of some tens of ns. The corresponding image frame 5 shows a faint glow at the rod during this period. Back discharges were not seen for the tested voltages when $h - a < 30\,\mathrm{cm}$.

B. Surface charge

In fig. 4a, the barrier is on the ground plane and the resulting surface potential is bell-shaped with maximum potential $\hat{U}_{\mathrm{S}} = 19\,\mathrm{kV}$, although it is not symmetric around $r = b$. Total calculated charge on the surface is $Q_{\mathrm{S}} = 934\,\mathrm{nC}$. Another experiment at the same voltage level, without leader-type channel inception, resulted in a bell-shaped distribution with $\hat{U}_{\mathrm{S}} = 11\,\mathrm{kV}$ and total charge $Q_{\mathrm{S}} = 682\,\mathrm{nC}$.

In fig. 4b, the surface potential is saddle-shaped, with a larger spread than in fig. 4a and 4b. The calculated surface charge density is also saddle-shaped, and negative right below the rod.

Measurements showed that the surface potential for all geometries was negligibly altered after about $1000\,\mathrm{min}$.

V. Discussion

A. Discharge development

1) Arrested leader-type channel: Leader-type channels typically cause breakdown of rod-plane gaps without barriers when they have propagated a few cm into the gap [18]. The local charging of the dielectric by the streamers at the channel front is likely reducing the field between the channel head and dielectric sufficiently to arrest the channel.

2) Back discharges: The back discharges are similar in frequency to the relaxation pulses observed by Blennow et al. [6] in a plane-parallel dielectric-covered electrode system under positive LI stress. The occurence and frequency of these restoring discharges depend upon the magnitude of surface charge, the insulation system geometry, the time derivative of the applied voltage and the amount of charge neutralized by each back discharge.

B. Surface charge

1) Shape: The higher capacitance of the surface when the barrier is closer to the ground plane leads to a narrower surface potential for similar charge distributions. Charge distributions will likely also be narrower with the barrier on the ground plane due to lower tangential field strengths supporting streamer propagation.

Leader-type channel propagation as in fig. 4a will influence the charge distribution, as streamers propagating from the channel head also charge the dielectric surface. Leader-type channel development therefore results in potential distributions that are greater in magnitude and less symmetric around $r = b$.

2) Condition for back discharges: Back discharges start when the surface charge induced field is high enough [6]. A rod-plane gap with rod radius $3.5\,\mathrm{mm}$ has a streamer onset voltage at positive polarity of around $U_{\mathrm{inc,pos}} = 20\,\mathrm{kV}$ [18]. Assuming a similar inception voltage magnitude for a streamer at negative impulse, the potential drop between the rod and barrier would be $U_{\mathrm{inc,neg}} = -20\,\mathrm{kV}$ at t_{back} in fig. 4b. Since the voltage at the rod is $U(t_{\mathrm{back}}) = 24\,\mathrm{kV}$, the maximum potential on the barrier at t_{back} should be around

$$U_{\mathrm{S},t_{\mathrm{back}}}(b) = U(t_{\mathrm{back}}) - U_{\mathrm{inc,neg}} = 44\,\mathrm{kV} \tag{2}$$

As back discharges in fig. 4b are observed even when the rod potential is approximately 0, it is possible that the surface potential is depleted such that $U_{\mathrm{S}}(b) < 20\,\mathrm{kV}$, in line with measurements.

Back discharges will likely continue until the potential between the barrier and rod is smaller than inception voltage

$$U_{\mathrm{S,after}}(b) < |U_{\mathrm{inc,neg}}| \tag{3}$$

Relation (3) can then be used as a rough estimate of the maximum residual potential below the rod after an impulse.

3) Surface charge density polarity: The surface charge density estimation method (1) results in negative surface charge density at the center when the barrier is closer to the rod, see fig. 4b. Although some charge on the barrier will be neutralized by the back discharges, the surface charge density should not change polarity locally. The local negative surface charge density could be a result of measurement errors.

VI. Conclusions

Surface charging of dielectrics depends upon the discharge mechanisms in play. In this work, a $60\,\mathrm{mm}$ positive LI stressed rod-plane gap with a dielectric barrier has been studied. The discharges were examined with high-speed images, PMTs and current and surface potential measurements. Three discharge phenomenons were observed: primary streamers, leader-type channels and back discharges. Whenever there is discharge activity, it always starts with primary streamers. These lead to a bell-shaped surface potential on the barrier. Leader-type channels develop at voltages closer to breakdown levels. Streamers from the front of these channels charge the surface additionally locally. It is suggested that the field from this charge is responsible for arresting the channel development.

Back discharges are observed at the impulse tail as regular pulses of 100–300 kHz. They are seen when the barrier is closer to the rod, as the reversed field becomes stronger. Back discharges will neutralize surface charge until the voltage drop between barrier and rod is lower than the rod inception voltage. As this voltage is approximately constant for a given rod radius, maximum surface potential after an impulse is restricted by the rod geometry.

ACKNOWLEDGMENT

This work is part of the project "Electrical insulation with low-GWP gases" (project number: 245422) funded by the Research Council of Norway and the industrial partners ABB AS, Norway and ABB Switzerland Ltd.. The authors would also like to thank Dag Linhjell at SINTEF Energy Research, Norway, for all his help with the experimental set-up.

REFERENCES

[1] F. Mauseth, A. Nysveen, and E. Ildstad, "Charging of dielectric barriers in rod-plane gaps," in *Proceedings of the 2004 IEEE International Conference on Solid Dielectrics, 2004. ICSD 2004*, vol. 1, Jul. 2004, pp. 447–451 Vol.1.

[2] S. Kumara, Y. Serdyuk, and S. Gubanski, "Charging of Polymeric Surfaces by Positive Impulse Corona," *IEEE Transactions on Dielectrics and Electrical Insulation*, vol. 16, no. 3, pp. 726–733, Jun. 2009.

[3] M. Sjöberg, Y. V. Serdyuk, S. M. Gubanski, and M. . S. Leijon, "Experimental study and numerical modelling of a dielectric barrier discharge in hybrid air–dielectric insulation," *Journal of Electrostatics*, vol. 59, no. 2, pp. 87–113, Sep. 2003.

[4] D. Durocher, M. Haim, L. Connor, and J. de Jong, "Safety by design: Solid insulated technologies challenge the use of SF6 in medium-voltage switchgear," in *Electrical Safety Workshop (ESW), 2015 IEEE IAS*, Jan. 2015, pp. 1–9.

[5] H. J. M. Blennow, M. L. A. Sjoberg, M. A. S. Leijon, and S. M. Gubanski, "Electric field reduction due to charge accumulation in a dielectric-covered electrode system," *IEEE Transactions on Dielectrics and Electrical Insulation*, vol. 7, no. 3, pp. 340–345, Jun. 2000.

[6] H. J. M. Blennow, M. . S. Leijon, and S. M. Gubanski, "Active high voltage insulation," *Journal of Electrostatics*, vol. 55, no. 2, pp. 159–172, Jun. 2002.

[7] S. M. Lebedev, O. S. Gefle, and Y. P. Pokholkov, "The barrier effect in dielectrics: the role of interfaces in the breakdown of inhomogeneous dielectrics," *IEEE Transactions on Dielectrics and Electrical Insulation*, vol. 12, no. 3, pp. 537–555, Jun. 2005.

[8] F. Mauseth, J. S. Jørstad, and A. Pedersen, "Streamer inception and propagation for air insulated rod-plane gaps with barriers," in *2012 Annual Report Conference on Electrical Insulation and Dielectric Phenomena (CEIDP)*, Oct. 2012, pp. 739–732.

[9] H. K. Meyer, F. Mauseth, A. Pedersen, and J. Ekeberg, "Streamer propagation in rod-plane air gaps with a dielectric barrier," Oct. 2016, pp. 1037–1040.

[10] Y. Chen, Y. Zheng, and X. Miao, "AC breakdown characteristics of air insulated point-plane gaps with polycarbonate barriers," in *2016 IEEE International Conference on High Voltage Engineering and Application (ICHVE)*, Sep. 2016, pp. 1–4.

[11] A. Kumada, S. Okabe, and K. Hidaka, "Residual charge distribution of positive surface streamer," *Journal of Physics D: Applied Physics*, vol. 42, no. 9, p. 095209, 2009.

[12] D. Faircloth and N. Allen, "High resolution measurements of surface charge densities on insulator surfaces," *IEEE Transactions on Dielectrics and Electrical Insulation*, vol. 10, no. 2, pp. 285–290, Apr. 2003.

[13] J. Deng, S. Matsuoka, A. Kumada, and K. Hidaka, "The influence of residual charge on surface discharge propagation," *Journal of Physics D: Applied Physics*, vol. 43, no. 49, p. 495203, 2010.

[14] I. Gallimberti, G. Marchesi, and L. Niemeyer, "Streamer corona at an insulator surface," in *7th international symposium on High voltage engineering*, 1991, pp. 26–30.

[15] M. Schueller, R. Gremaud, and C. Franck, "Accuracy of surface potential measurements of HVDC spacers," in *2014 International Conference on High Voltage Engineering and Application (ICHVE)*, Sep. 2014, pp. 1–4.

[16] A. Winter and J. Kindersberger, "Stationary resistive field distribution along epoxy resin insulators in air under DC voltage," *IEEE Transactions on Dielectrics and Electrical Insulation*, vol. 19, no. 5, pp. 1732–1739, Oct. 2012.

[17] T. Kitamura, H. Kojima, N. Hayakawa, K. Kobayashi, T. Kato, and T. Rokunohe, "Influence of space charge by primary and secondary streamers on breakdown mechanism under non-uniform electric field in air," in *2014 IEEE Conference on Electrical Insulation and Dielectric Phenomena (CEIDP)*, Oct. 2014, pp. 122–125.

[18] H. K. H. Meyer, F. Mauseth, A. Pedersen, M. Husøy, and J. Ekeberg, "Breakdown in short rod-plane air gaps under positive lightning impulse stress," in *Nordic Insulation Symposium (Nord-IS)*, 2017.

[19] H. Kojima, K. Hotta, T. Kitamura, N. Hayakawa, A. Otake, K. Kobayashi, T. Kato, T. Rokunohe, and H. Okubo, "Classification of impulse breakdown mechanisms under non-uniform electric field in air," *IEEE Transactions on Dielectrics and Electrical Insulation*, vol. 23, no. 1, pp. 194–201, Feb. 2016.

[20] S. Kumara, "Electrical Charges on Polymeric Insulator Surfaces and their Impact on Flashover Performance," Doctoral thesis, Chalmers University of Technology, 2012.

[21] M. A. Noras, "Non-contact surface charge/voltage measurements: capacitive probe—principle of operation," *Trek Application Note*, no. 3001, pp. 1–8, 2002.

[22] S. Okabe and A. Kumada, "Measurement Methods of Accumulated Electric Charges on Spacer in Gas Insulated Switchgear," *IEEE Transactions on Power Delivery*, vol. 22, no. 3, pp. 1547–1556, Jul. 2007.

[23] J. Kindersberger and C. Lederle, "Surface charge decay on insulators in air and sulfurhexafluorid - part I: simulation," *IEEE Transactions on Dielectrics and Electrical Insulation*, vol. 15, no. 4, pp. 941–948, Aug. 2008.

[24] J. E. Mark, *Polymer data handbook*. Oxford University Press, 2009.

[25] M. Noras and A. Pandey, "Evaluation of Surface Charge Density with Electrostatic Voltmeter - Measurement Geometry Considerations," in *IEEE Industry Applications Society Annual Meeting, 2008. IAS '08*, Oct. 2008, pp. 1–6.